Desalination and Water Treatment
www.deswater.com
doi: 10.5004/dwt.2021.27767

241 (2021) 64–73
November

Photocatalytic performance of $BiVO_4$/RGO composite for degradation of Orange II under visible light

Mengyao Luo, Xue Sun, Tingting Jiao, Guangzhou Qu*

College of Natural Resources and Environment, Northwest A&F University, Yangling, Shaanxi Province 712100, PR China, Tel. +86-02987080050; email: qugz@nwsuaf.edu.cn.cn (G. Qu), Tel. +86-15808249393; email: 979858444@qq.com (M. Luo), Tel. +86-15229089987; email: 1101118205@qq.com (X. Sun), Tel. +86-19591282532; email: 1351213670@qq.com (T. Jiao)

Received 20 April 2021; Accepted 5 September 2021

ABSTRACT

A simple hydrothermal method was employed to synthesize $BiVO_4$ supported on reduced graphene oxide ($BiVO_4$/RGO) composite photocatalyst to enhance photocatalytic activity of $BiVO_4$ for degradation of dye wastewater under visible light. The prepared photocatalysts were characterized by scanning electron microscopy, transmission electron microscopy, X-ray diffraction, Fourier transform infrared spectroscopy, X-ray photoelectron spectroscopy, UV-Vis DRS and photocurrent measurements. The photocatalytic performances of the $BiVO_4$/RGO composite were evaluated by degradation of Orange II (AO7) under visible light irradiation (λ > 420 nm). A series of experiments were carried out to evaluate the effects of various factors on removal efficiency of AO7. The results show that the $BiVO_4$/RGO composite exhibited much higher photocatalytic activity than pure $BiVO_4$. The highest removal efficiency of AO7 was obtained, and reach 100% after 150 min when the doping content, pH value, catalyst dosage was GB30 (30 mg of GO corresponds to 1 mmol of $BiVO_4$), pH = 9 and 200 mg, respectively. The free radical trapping experiments show that $^\bullet O_2^-$ played the most important role in the degradation of AO7. The enhanced catalytic activity of the $BiVO_4$/RGO composite can be attributed to the RGO. As an electron acceptor and transporter, RGO can effectively promote charge transfer in composite and inhibit the recombination of photo-induced electron-hole pairs.

Keywords: $BiVO_4$; Reduced graphene oxide; Photocatalytic; Dye wastewater; Degradation

1. Introduction

Visible light-responsive photocatalytic technology is recognized as one of the most potential wastewater treatment technologies due to its non-toxicity, low investment cost, good chemical stability and other advantages [1–4]. $BiVO_4$, as a visible light-responsive photocatalyst, has attracted wide attention due to its narrow band gap (2.4 eV) and excellent photocatalytic activity under visible light irradiation [5,6]. Unfortunately, $BiVO_4$ still has some defects, such as poor adsorption performance and the difficulty in migration of photo-generated electron-hole pairs, which seriously restricts photocatalytic performance of $BiVO_4$ for the degradation of organic pollutants in wastewater [3].

In order to solve these problems, many attempts have been made to enhance the photocatalytic activity of $BiVO_4$, in which doping other substances is considered a good option [7–9]. Graphene is a carbonaceous material that is closely arranged into a two-dimensional honey-comb lattice structure by a single layer of carbon atoms, which has a variety of extraordinary properties because of its unique nanostructure [10]. When graphene is incorporated into the semiconductor nanocomposite, the abundant delocalized electrons in the conjugated sp^2-bonded carbon network of graphene enhance the transport of photo-generated electrons, which

* Corresponding author.

in turn promotes the efficiency of photocurrent conversion. In addition, graphene has high electrical conductivity and large surface area, thereby suppressing the recombination of photo-induced electron-hole pairs, and significantly enhancing electron transfer [9,11,12]. In view of this, compositing $BiVO_4$ with graphene is a promising measure to overcome the disadvantages of pure $BiVO_4$. Many methods have been developed for the preparation of $BiVO_4$/graphene composite involving aqueous process, sol-gel method, microwave-assisted approach, metalorganic decomposition technique and hydrothermal method [13–16], in which hydrothermal method has aroused widespread concern because of its capability to synthesize photocatalyst with perfect crystal structures and regular shapes in an environmentally friendly way. However, current hydrothermal methods still call for complex process and strict synthesis condition, which greatly blocks its practical application.

In this study, a simple and high efficiency hydrothermal method was employed to synthesize $BiVO_4$ supported on reduced graphene oxide ($BiVO_4$/RGO) composite. The morphology, crystalline, structural and photo-electronic property of the $BiVO_4$/RGO photocatalyst were characterized by scanning electron microscopy (SEM), transmission electron microscopy (TEM), X-ray diffraction (XRD), Fourier transform infrared spectroscopy (FTIR), X-ray photoelectron spectroscopy (XPS) and UV-Vis diffuse reflectance spectroscopy (UV-Vis DRS) and photocurrent measurements. The photocatalytic activity of as-prepared $BiVO_4$/RGO composite was evaluated by the degradation of Orange II (AO7) under visible light irritation. The effects of various factors (doping content of GO, pH of precursor fluid, catalyst dosage and initial solution concentration) on AO7 removal were investigated. Meanwhile, in order to testify the existence of various radicals and compare its roles in the degradation of AO7, a set of radical trapping experiments were carried out. Finally, the photocatalytic degradation mechanism of $BiVO_4$/RGO composite to AO7 was proposed.

2. Experimental

2.1. Materials and reagents

Graphite powder, as the precursor of graphene oxide (GO), was obtained from Tianjin Tianli Chemical Reagent Co., Ltd., (China). Bismuth nitrate pentahydrate ($Bi(NO_3)_3·5H_2O$) and ammonium vanadate (NH_4VO_3) were obtained from Aladdin and Shanghai Shanpu Chemical Co., Ltd. (China), respectively. Other chemicals were analytical grade and used as received without further purification.

2.2. Preparation of $BiVO_4$/RGO composite

GO was prepared by the modified Hummers method [17,18]. In a typical synthesis of $BiVO_4$/RGO composite, firstly, 90 mg of GO was dispersed into 40 mL of mixed solution of de-ionized water and absolute ethanol at the ratio of 1:1 with sonication for 1 h. Secondly, 0.54 g of $Bi(NO_3)_3·5H_2O$ and 0.129 g of NH_4VO_3 were separately added into 20 mL absolute ethanol with stirring over 1 h at room temperature. Then, mixed the three solutions together, adjusted the pH to 9 with ammonia solution and stirred for 30 min. Finally, the resulting mixture was transferred into two 50 mL Teflon-lined stainless steel autoclaves and heated to 180°C for 6 h. After the reaction mixture was cooled to room temperature, filtered it, washed with de-ionized water for five times, and dried in a vacuum oven at 60°X for 12 h. The obtained composite was $BiVO_4$/RGO. Adjusted the content of GO to get different products. Same processes were used to synthesize pure $BiVO_4$ without RGO.

2.3. Characterization methods

The surface morphologies and microstructures of the composites were investigated by SEM (Nova nanosem430) and TEM (JEM-2100F), respectively. The crystalline phases of the prepared samples were identified by XRD (X'Pert PRO MPD) with CuKα radiation and the scanning angle ranged from 5° to 70° of 2θ. FTIR and XPS spectrometer were used to analyze the chemical bonds and composition information of samples. FTIR spectra were measured on a BRUKER Vetex70 FTIR spectrometer with KBr pellets as the sample matrix in the 400–4000 cm^{-1} region. XPS spectra were carried out on PHI-5000 Versaprobe with Mg Kα radiation. UV-Vis DRS were obtained using a PE lambda 750S in the wavelength range of 200 to 800 nm to characterize the optical properties of the photocatalysts. The transient photocurrent was performed on an electrochemical analyzer CHI760E.

2.4. Photocatalytic experiment

Photocatalytic activity of $BiVO_4$/RGO composite was determined by AO7 removal under visible light irradiation. The 300 W xenon lamp was used as the light source and the UV filter was used to remove the radiation below 420 nm. Under without special statement, 0.1 g of photocatalyst was added to 200 mL of 20 mg/L AO7 aqueous solution. Before starting the illumination, the reaction mixture was stirred for 30 min in the dark in order to reach the adsorption-desorption equilibrium between the dye and photocatalyst. The suspension was sampled at certain time intervals and filtered through 0.22 μm filters to removal catalyst powder, and finally analyzed using a UV-Vis spectrophotometer at 486 nm.

3. Results and discussion

3.1. Morphology and microstructure

The surface morphology and microstructure of photocatalyst affect its photocatalytic activity. Fig. 1 shows the typical SEM and TEM images of $BiVO_4$ and $BiVO_4$/RGO composites. As shown in Fig. 1a, $BiVO_4$ has many coral-like short rod particles which were evenly distributed in size and combine with each other, but are still relatively loose and not concentrated. From Fig. 1b it can be seen that the aggregate phenomenon of $BiVO_4$/RGO composite is more obvious, and the coral-like short rod particles are arranged more closely and the degree of polymerization become higher than that in Fig. 1b. It is obvious that coral-like short rod $BiVO_4$ particles which are assembled by irregular flakes, attached to the RGO sheet. From the TEM images of $BiVO_4$/RGO composite, the RGO can be clearly observed, and $BiVO_4$ is evenly distributed on the RGO surface. Fig. 1c shows that the coral-like short rod particles mentioned above. The relatively

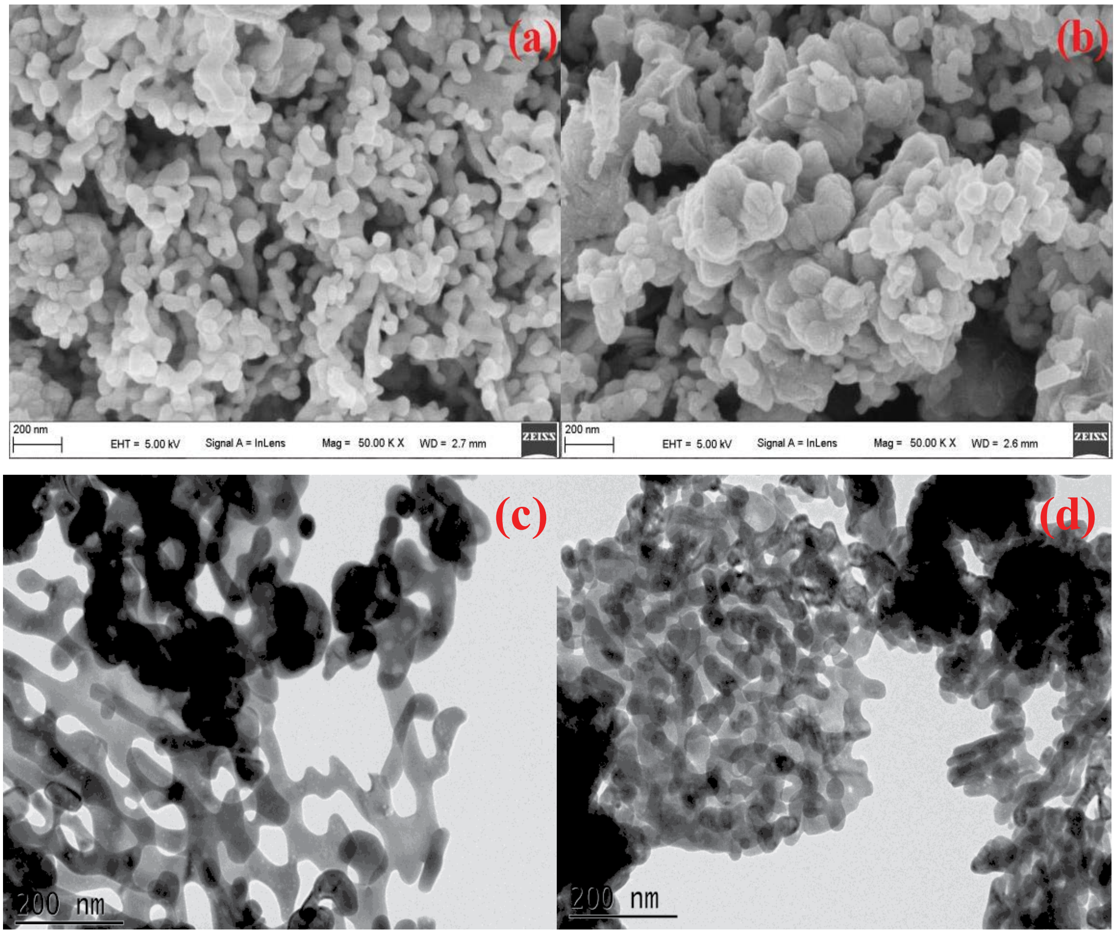

Fig. 1. The SEM and TEM images of samples. (a) SEM image of $BiVO_4$, ×50,000, (b) SEM image of $BiVO_4$/RGO, ×50,000, (c) TEM images of $BiVO_4$, ×50,000, and (d) TEM images of $BiVO_4$/RGO, ×50,000.

loose structures which they polymerize are indeed present. The size of coral-like short rod particles is about 200 nm. There are quite a few particles combined with RGO to form a new structure and has a butterfly-like shape, as shown in Fig. 1d. The above results can fully demonstrate that $BiVO_4$ is indeed combined with RGO.

3.2. Crystal structure

Fig. 2 shows the XRD diffraction patterns of the GO, $BiVO_4$ and $BiVO_4$/RGO. It is confirmed that all the photocatalysts have a single monoclinic-scheelite structure and their diffraction peaks can be assigned to monoclinic $BiVO_4$ (JCPDS NO.14-0688) [6]. However, the typical diffraction peak of GO (0 0 1) cannot be observed in the XRD pattern of $BiVO_4$/RGO. Studies have shown that, if the regular stack of GO is destroyed, for example, by exfoliation, their diffraction peaks become weak or even disappear. In addition, GO can be reduced during the hydrothermal reaction in the presence of alcohols, while the exfoliated RGO sheets show no peak of (0 0 1). It is also possible that the relatively high content and good crystallinity of $BiVO_4$ in the composite generate strong diffraction peaks, covering the diffraction of the carbon sheets [19].

3.3. FTIR spectra

The FTIR absorption spectrums of the GO, $BiVO_4$ and $BiVO_4$/RGO samples were analyzed to study the bond vibrational chemistry present within the materials (Fig. 3). The GO spectrum shows the presence of various oxygen-containing groups, including the absorption peaks O–H stretching vibration of water molecules adsorbed on the GO surface (3,400 cm^{-1}), C=O stretching vibrations of the COOH groups (1,720 cm^{-1}), O–H deformation vibrations of the COOH groups (1,630 cm^{-1}) and C–O stretching vibrations of the epoxy groups (1,065 cm^{-1}) [19]. Compared with $BiVO_4$/RGO, it can be clearly seen that almost all the characteristic peaks of GO disappeared for $BiVO_4$/RGO, suggesting that GO in $BiVO_4$/RGO has been reduced.

3.4. XPS spectra

The chemical composition of $BiVO_4$/RGO composite was further investigated by the XPS spectra (Fig. 4). As shown in Fig. 4a, signals from primary elemental composition of Bi, V, O and C are clearly observed, determining the definite existence of $BiVO_4$ and carbon content in the sample. The Bi 4f XPS spectrum of the sample is shown in Fig. 4b. XPS signals

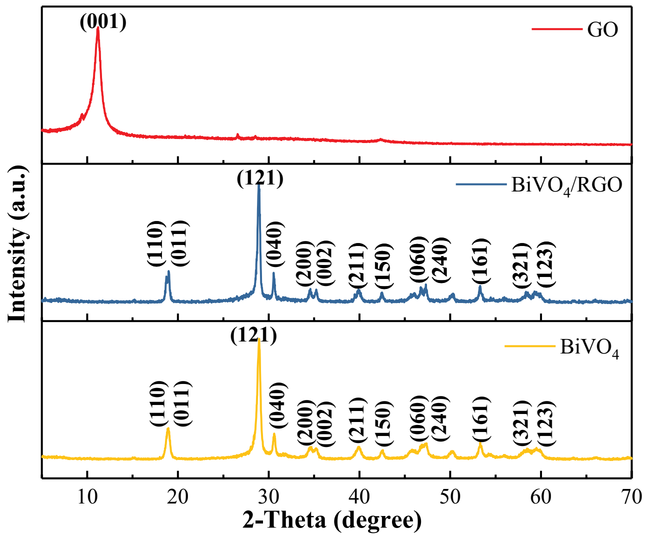

Fig. 2. XRD patterns of GO, $BiVO_4$ and $BiVO_4$/RGO samples.

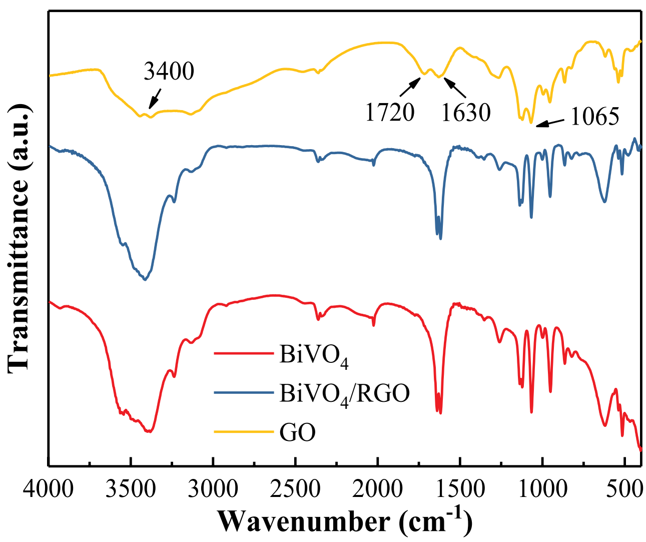

Fig. 3. The FTIR absorption spectrums of the GO, $BiVO_4$ and $BiVO_4$/RGO samples.

of Bi 4f are located at binding energies at about 159.37 eV (Bi $4f_{7/2}$) and 164.67 eV (Bi $4f_{5/2}$) respectively, attribute to Bi^{3+} bismuth state [20]. The V 2p peak in Fig. 4c are centered at 517.07 eV (V $2p_{3/2}$) and 524.67 eV (V $2p_{1/2}$), ascribed to V^{5+} [21]. The O 1s peak is shown in Fig. 4d, which is fitted into the peak centering at 530.17 eV and mainly assigned to the oxygen in the prepared sample lattice [20]. The C 1s XPS spectrum of the $BiVO_4$/GO sample is shown in Fig. 4e. Three types of carbon bonds, C–C species (284.77 eV), C–OH species (285.67 eV), and C=O–OH species (288.37 eV), are apparently detected in $BiVO_4$/GO samples [22].

3.5. UV-Vis DRS spectra

UV-Vis DRS spectra are used to characterize the optical properties of the semiconductor photocatalysts. As shown in Fig. 5, strong absorption characteristics in the UV region and a broad adsorption band from 200 to 480 nm is observed for $BiVO_4$. $BiVO_4$ exhibits an absorption edge at around 510 nm, showing good visible light response. For the $BiVO_4$/RGO composite, the absorption edge shifted to around 590 nm, and the light absorption ability in the range of 550 to 800 nm is also increased due to the absorption of RGO. According to the optical absorption theory of crystal materials, the band gap energy of the composite is quantitatively calculated. The electron corresponding to the absorption edge is excited to jump from the top of the valence band to the bottom of the conduction band. The nature of the band structure can be explored and the optical energy gap can be obtained by analyzing the absorption edge. There is the following relationship between the absorption coefficient and the energy of hν of the incident photon:

$$\left(\alpha h\nu\right)^2 = A\left(h\nu - E_g\right) \quad (1)$$

where α, h, ν, A and E_g represent the absorption coefficient, Planck's constant, optical frequency, constant, and bandgap energy, respectively.

The bandgap energy (E_g) of $BiVO_4$ and $BiVO_4$/RGO composite can be estimated. The bandgap energy of $BiVO_4$, $BiVO_4$/RGO is 2.51 eV and 2.38 eV respectively. The results further demonstrate that the introduction of RGO can change the electronic structure of $BiVO_4$ in $BiVO_4$/RGO composite, thereby reducing the bandgap of $BiVO_4$/RGO, broadening the optical response range, improving photocatalytic performance [10,23].

3.6. Transient photocurrent responses

To investigate the photo-electronic properties of $BiVO_4$/RGO composites, the transient photocurrent response were tested, and shown in Fig. 6. The corresponding photocurrent densities were calculated to be 0.048 and 0.12 μA/cm^2 for $BiVO_4$ and $BiVO_4$/RGO samples, respectively. $BiVO_4$/RGO possessed the largest photocurrent (more than 2.5 times of $BiVO_4$ sample). The enhanced photocurrent density was obviously attributed to the faster electron migration and less recombination of the photo-produced electron-hole pairs [24]. The order of photocurrent densities of as-prepared photocatalysts proved that integration RGO nanosheets with $BiVO_4$ could promote separation and migration of the charges.

3.7. Photocatalytic activity and influential factors

To evaluate the effects of various factors (doping content of GO, pH of precursor fluid catalyst dosage and initial solution concentration) on the removal efficiency of AO7, a series of experiments were carried out under various conditions. The mass ratio of GO and $BiVO_4$ affects the electron transfer ability of $BiVO_4$/RGO composite and separation efficiency of photo-generated electron-hole pairs, which affect its photocatalytic activity. The effects of mass ratio of GO and $BiVO_4$ on photocatalytic performance of $BiVO_4$/RGO composite to AO7 removal is shown in Fig. 7. According to the ratio of GO and $BiVO_4$, the samples obtained were named GB10, GB20, GB30, GB40, GB50 and

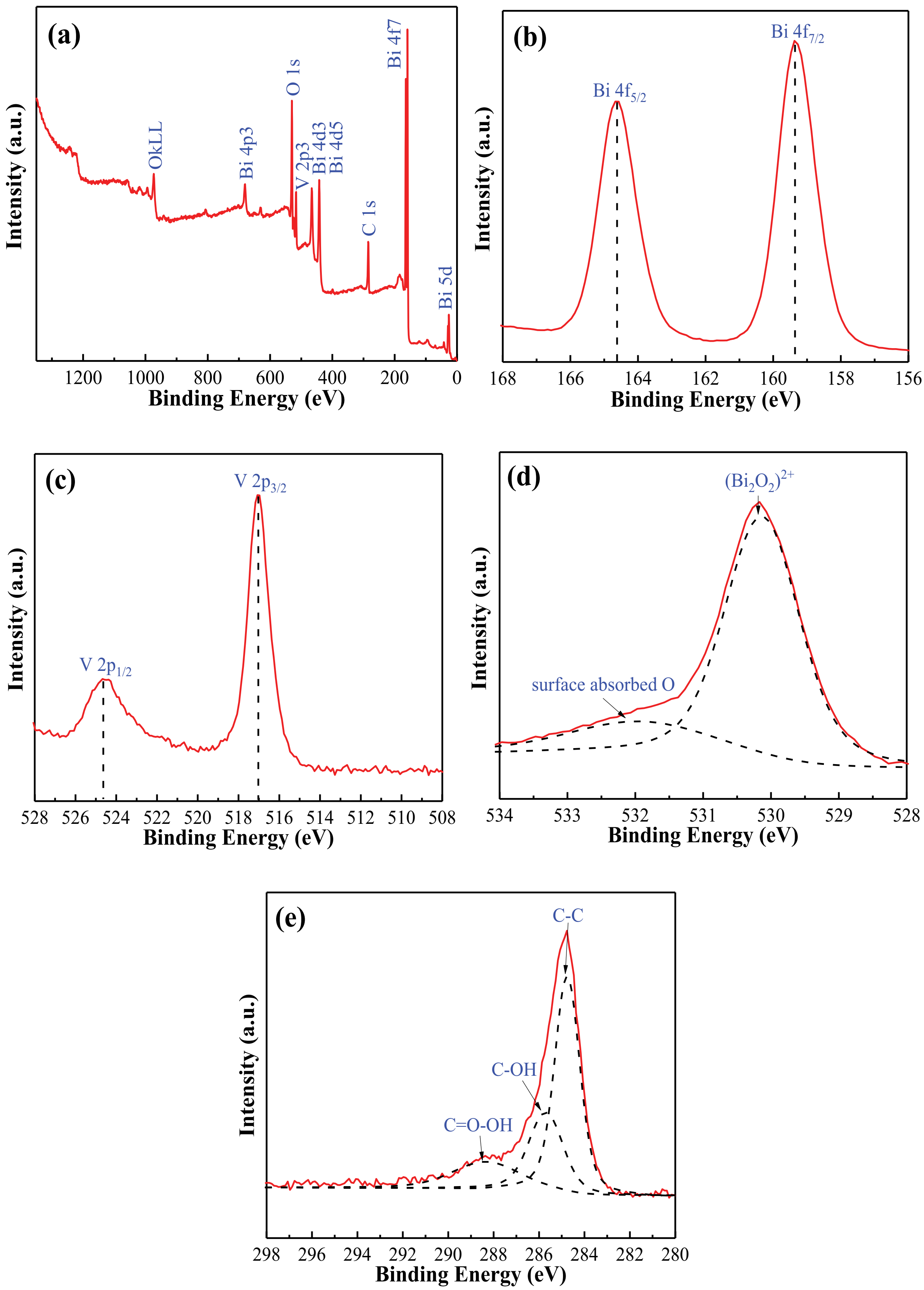

Fig. 4. The XPS spectrum of $BiVO_4$/RGO composite: (a) full range, (b) Bi 4f, (c) V 2p, (d) O 1s, and (e) C 1s.

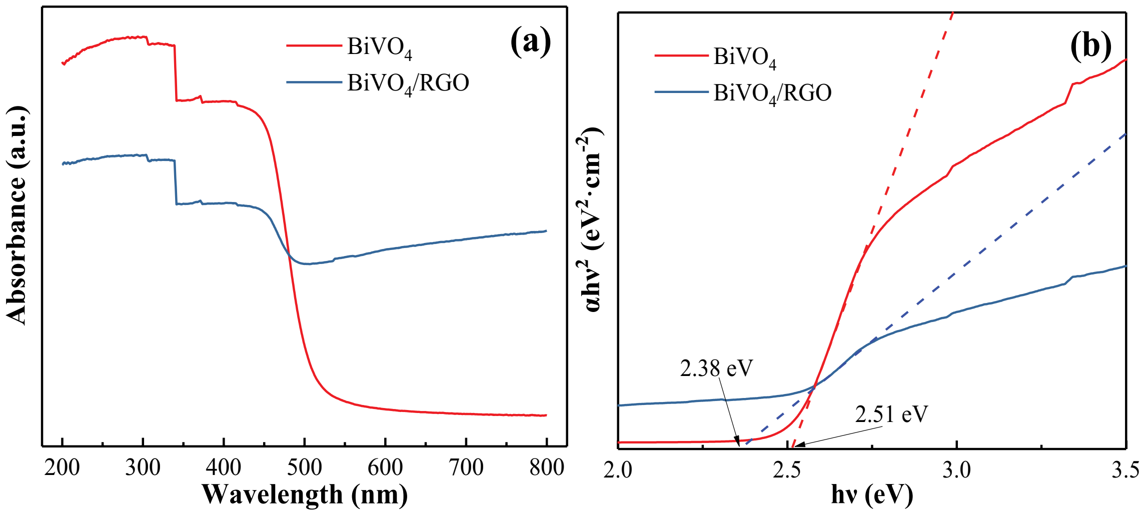

Fig. 5. UV-Vis spectra (a) and plots of (hν)^2 vs. hν (b) of $BiVO_4$ and $BiVO_4$/RGO composite.

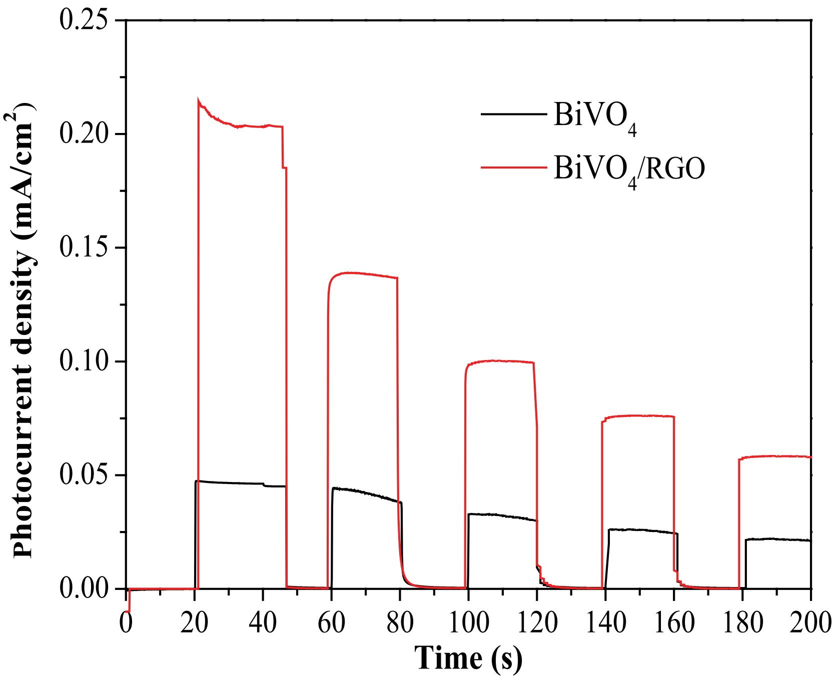

Fig. 6. Photocurrent responses of $BiVO_4$ and $BiVO_4$/RGO composite.

GB60, respectively. Take GB60 as an example, GB60 specifically means that 60 mg of GO corresponds to 1 mmol of $BiVO_4$. When the content of GO doping increased from GB10 to GB20, the photocatalytic efficiency increased gradually, which was 23.81% and 58.79%, respectively. When the doping content was GB30, the best catalytic effect was achieved, and the removal efficiency was 78.78%. As the content of GO doping continued to increase, the photocatalytic effect was inhibited. The removal efficiency of AO7 was reduced to 67.25%, 46.62% and 26.70%, respectively. The reason is that RGO has excellent electron transfer ability. It can rapidly transfer photo-generated electrons on the surface of $BiVO_4$, inhibit the recombination of photo-generated electrons and hole, and enhance the photocatalytic activity of $BiVO_4$. The introduction of RGO which is reduced by GO in hydrothermal reaction is beneficial to improve the photocatalytic activity of the composite. With the increase of RGO content, the photocatalytic activity of the composite increases gradually. However, too much RGO will intensify the competition for light, so that the light acting on $BiVO_4$ will be less. The photocatalytic activity of the composite will be reduced.

Fig. 8 shows the photocatalytic efficiency curves of $BiVO_4$/RGO with different pH (=3, 5, 7, 9, 11) of precursor fluid to AO7. It can be seen that the removal efficiency of AO7 gradually become better with the increase of pH, the removal efficiency of AO7 is 66.32%, 74.02% and 78.78%,

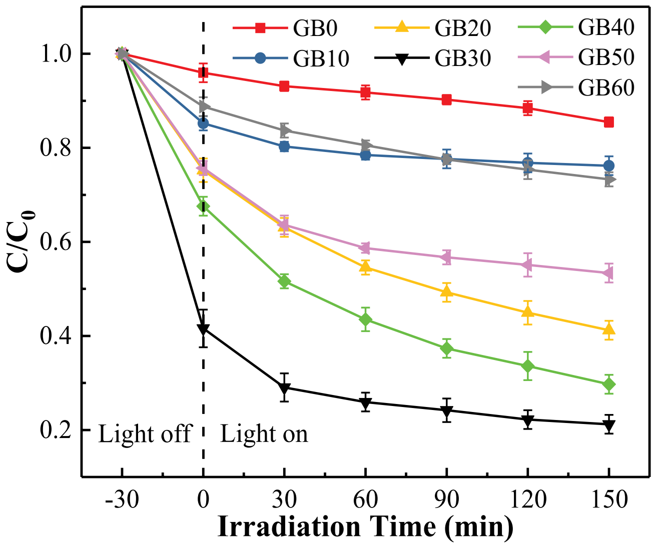

Fig. 7. Absorption and photocatalytic efficiency of $BiVO_4$ with different content of RGO to AO7.

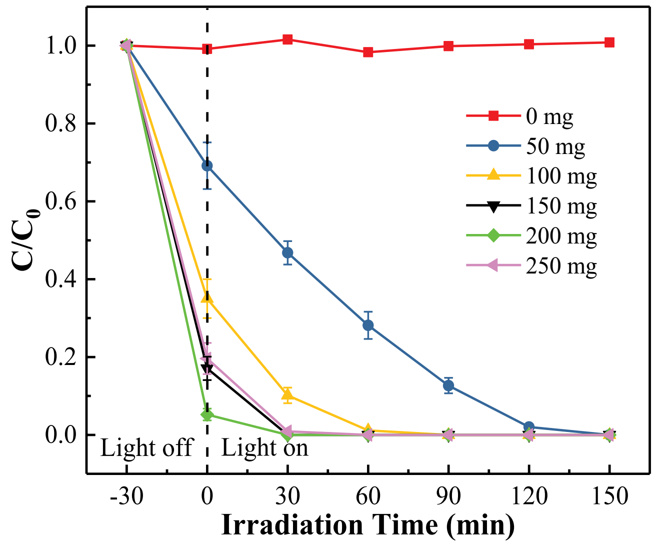

Fig. 9. Absorption and photocatalytic efficiency of different dosages of $BiVO_4$/RGO to AO7.

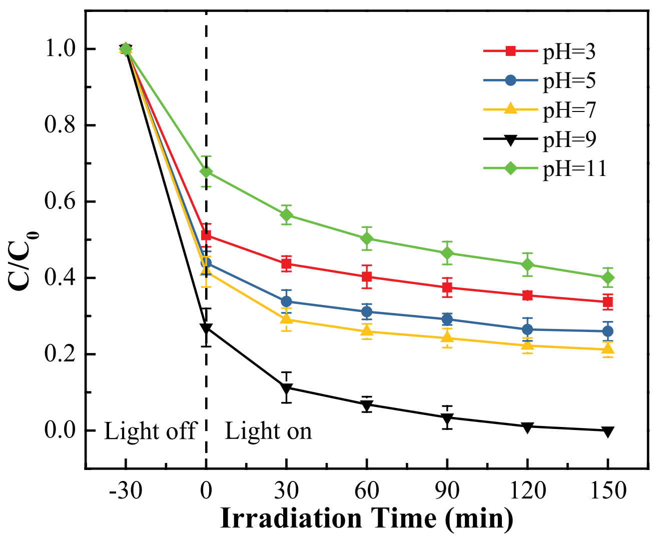

Fig. 8. Absorption and photocatalytic efficiency of $BiVO_4$/RGO to AO7 at different pH of precursor fluid.

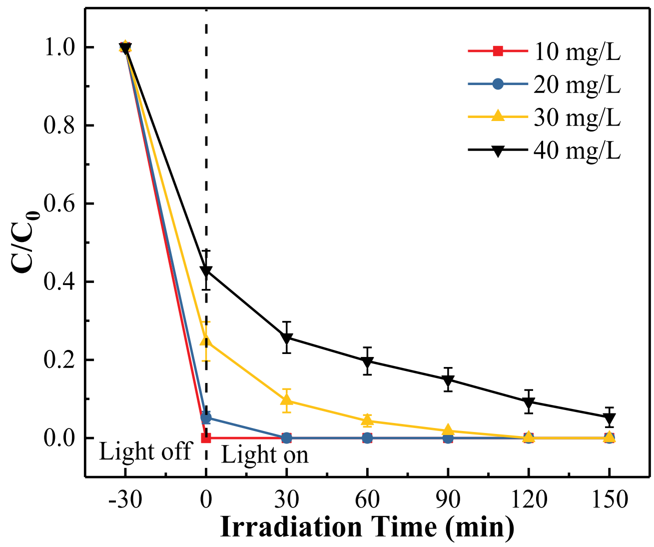

Fig. 10. Absorption and photocatalytic efficiency of $BiVO_4$/RGO to AO7 of different initial concentrations.

respectively. The removal is optimal at pH = 9, AO7 is almost removed completely. When the pH continues to increase, the removal efficiency of AO7 decreases, the removal efficiency of AO7 is only 59.94% at pH = 11. The composite material with different crystal forms can be selected by adjusting the pH of the precursor liquid. When the pH of reaction precursor liquid is gradually increased from acidity, the tendency of the product to transform to monoclinic crystal form is also enhanced [25].

Fig. 9 shows the effects of catalyst dosage on the removal efficiency of AO7. The removal efficiency of AO7 increased with the amount of the $BiVO_4$/RGO composite. When the amount of photocatalyst reached 200 mg, the removal efficiency of AO7 reached 100% after 30 min. With the increase of amount of photocatalyst, the active sites increase, thus promoting the adsorption of pollutants and improving the photocatalytic activity. When the catalyst is added too much, the absorption of light is saturated by the photocatalyst [26]. In addition, excessive catalyst increase the opacity and light scattering of AO7, resulting in less activated $BiVO_4$ molecules, and ultimately reduce removal efficiency of AO7 [27].

Fig. 10 shows the photocatalytic efficiency of $BiVO_4$/RGO under different AO7 initial concentrations. The initial concentration has profound effects on AO7 removal, and the removal efficiency of AO7 gradually decreases with the increase of initial concentration. When the initial concentration of AO7 was 20 mg/L, AO7 was almost removal completely after 30 min of illumination. When the initial concentration of AO7 was increased from 20 mg/L to

30 mg/L and 40 mg/L, it took 120 and 150 min to reach the ideal removal efficiency, respectively. Increasing the initial concentration of the solution while other conditions remain unchanged, that is, the active species in the photocatalytic reaction system do not increase. Therefore, the limited active species is not enough to remove more AO7 molecules [3]. In addition, the excess AO7 may occupy active sites or generate a filter effect, causing a hindrance for the generation of active radicals [28,29].

3.8. Photocatalytic mechanisms

Fig. 11 shows the UV-Vis spectra of AO7 with the change of visible light irradiation time. As shown in Fig. 11, AO7 dye molecules have two main absorption peaks at 306 and 486 nm wavelength, which represent benzene-like structures and azo bond respectively [27]. The intensity decreases with irradiation time. It is indicate that the benzene-like structures and azo bond of AO7 dye molecules are destroyed during photocatalytic reaction, and AO7 is gradually degraded. At the same time, no other absorption peaks appears, which indicate no new by-products are created in the wavelength range of 300 to 600 nm. The inset in Fig. 11 corresponds to the color change of the AO7 solution at different irradiation time. It can be seen from the inset that the color of the AO7 solution has become almost colorless after 120 min. It further confirms that the AO7 can be degraded by $BiVO_4$/RGO composite under visible light.

Decolorization of AO7 does not mean complete mineralization. Chemical oxygen demand (COD) is an important indicator to reflect the relative content of organic matter in wastewater. It can help us to understand the degree of mineralization of AO7 by analyzing the change of COD. As shown in Fig. 12, the COD content gradually decreases with the extension of the irradiation time. Compared with the results of Fig. 11, it is found that the color of AO7 solution tends to be colorless after 60 min, but the removal rate of COD only reaches 62.50%. When the treatment time is prolonged to 120 min, the absorbance value is close to 0, but the removal rate of COD only increases to 87.50%. It is concluded that AO7 dye molecule has not been completely mineralized in the process of photocatalytic reaction and some intermediate organic compounds still exist [26].

A large number of active radicals are generated in the photocatalytic process, among which $^{\bullet}O_2^-$, $^{\bullet}OH$ and h^+ are considered to be the three most important radicals. In order to testify the existence of these three radicals, and compare its roles in the degradation of AO7, a set of radical trapping experiments were carried out. In this study, p-benzoquinone (p-BQ), isopropyl alcohol (IPA) and ammonium oxalate (AO) were employed as radical capture agents to trap $^{\bullet}O_2^-$, $^{\bullet}OH$ and h^+, respectively. As shown in Fig. 13, the different capture reagents all show a few suppression effects on the degradation efficiency due to the competition for active radicals between the capture reagents and pollutant molecules. Fig. 13a shows the effects of different concentrations of p-BQ on AO7 degradation. When the solution system does not contain p-BQ, the removal efficiency of AO7 can reach 98.31% at 90 min. When the p-BQ concentration is increased from 0 to 0.1, 0.5 and 1 mmol/L, the removal efficiency of AO7 is reduced from 98.31% to 51.93%, 41.60% and 33.70%, respectively. It is indicated that $^{\bullet}O_2^-$ is involved in the photocatalytic process and participates in the photocatalytic degradation of AO7. Fig. 13b shows the effects of concentrations of IPA on photocatalytic degradation of AO7. When the concentration of IPA is increased from 0 to 0.1, 0.5 and 1.0 mmol/L, the removal efficiency of AO7 decreased by 35.02%, 38.51% and 40.61%, respectively, which is lower than that of p-BQ to AO7 degradation. Fig. 13c shows the effects of different concentrations of AO on degradation of AO7. As shown in Fig. 13c, when the AO concentration is increased, the degradation efficiency of AO7 did not decrease significantly, which indicate that there are h^+ productions during the photocatalytic process, but its effect is relatively weak. By comparing the results above, it can be found that $^{\bullet}O_2^-$ radical play more important role to the degradation of AO7.

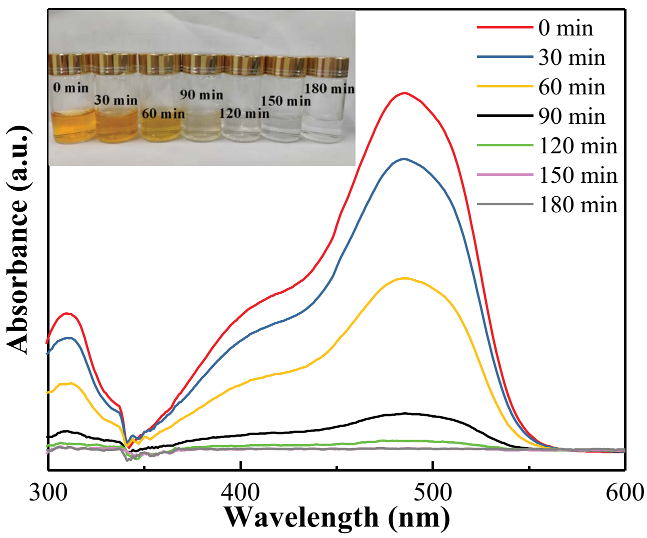

Fig. 11. UV-Vis spectra of AO7 after different irradiation time under visible light.

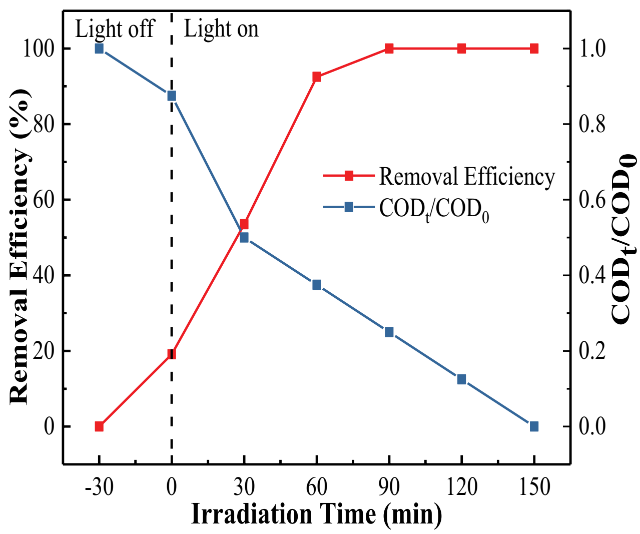

Fig. 12. The changes of removal efficiency of AO7 and COD after different irradiation time.

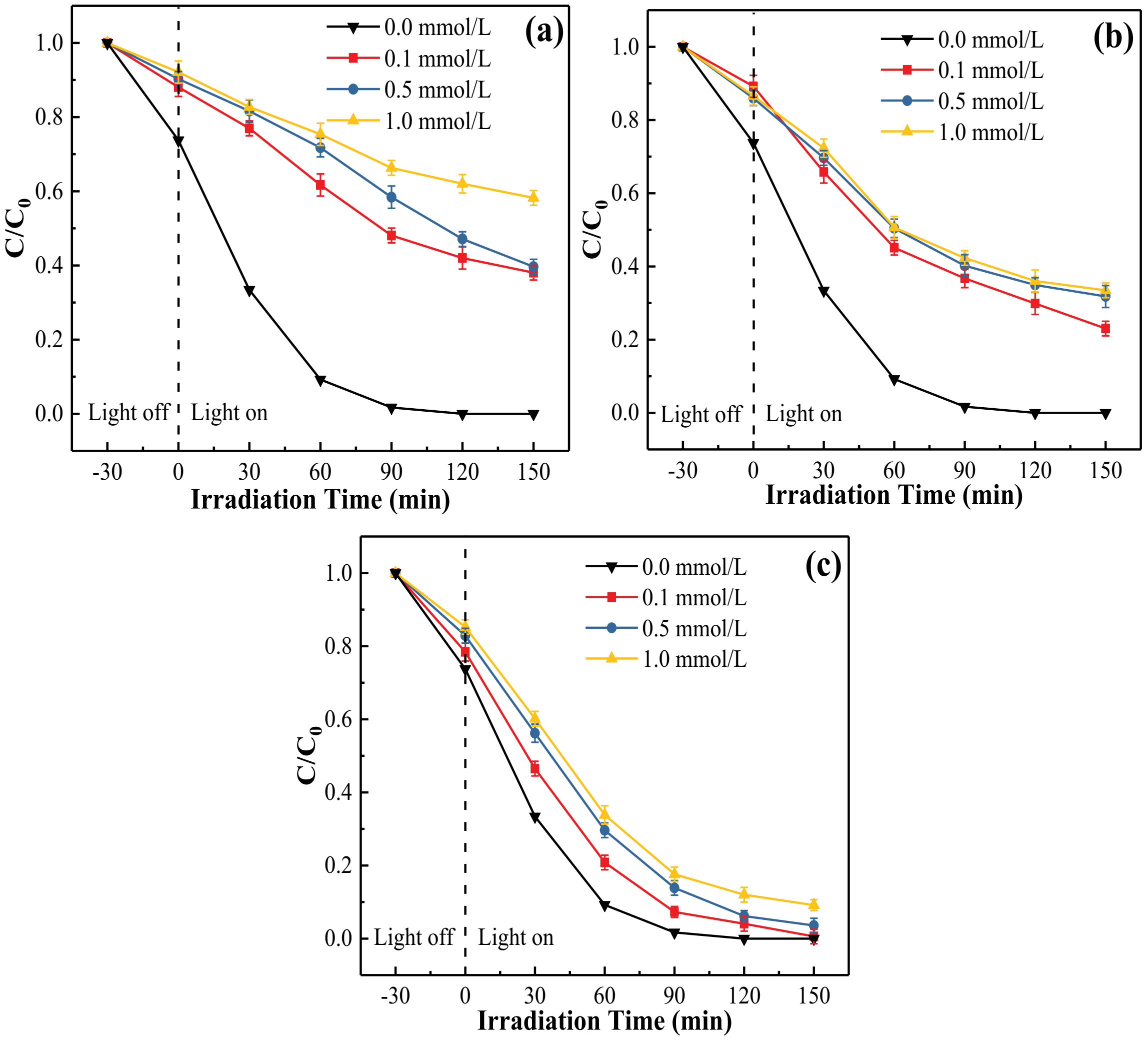

Fig. 13. The effects of different radical capture agents on photocatalytic degradation of AO7: (a) p-BQ, (b) IPA, and (c) AO.

To sum up, a series of degradation experiments demonstrate that the RGO in $BiVO_4$/RGO composite can improve photocatalytic activity by promoting charge transfer and separation. Firstly, electron-hole pairs are excited within $BiVO_4$ upon irradiation. Then, the electrons are transferred quickly from the conduction band (CB) of $BiVO_4$ to the surfaces of the RGO and consumed by dissolved oxygen to yield $^{\bullet}O_2^-$, which can react with H_2O/H^+ to form $^{\bullet}OH$. Meanwhile, the holes on the valence band (VB) of $BiVO_4$ can oxidize H_2O/OH^- to also form $^{\bullet}OH$ [30–33]. $^{\bullet}O_2^-$ and holes equipped with strong oxidizability also can oxidize AO7 molecules [30]. The specific reactions involved in the process are summarized as follows:

$$BiVO_4 + hv \rightarrow BiVO_4\left(e^- + h^+\right) \tag{2}$$

$$BiVO_4\left(e^-\right) + RGO \rightarrow RGO\left(e^-\right) \tag{3}$$

$$RGO\left(e^-\right) + O_2 \rightarrow RGO + {}^{\bullet}O_2^- \tag{4}$$

$${}^{\bullet}O_2^- + H_2O / H^+ \rightarrow {}^{\bullet}OH \tag{5}$$

$$BiOV_4\left(h^+\right) + H_2O / OH^- \rightarrow {}^{\bullet}OH \tag{6}$$

$${}^{\bullet}O_2^- / {}^{\bullet}OH / BiOV_4\left(h^+\right) + AO7 \rightarrow CO_2 + H_2O \tag{7}$$

4. Conclusion

In this study, the $BiVO_4$/RGO composite photocatalyst was successfully prepared by hydrothermal synthesis method. The prepared $BiVO_4$/RGO composite showed higher photocatalytic activity than pure $BiVO_4$. The highest removal efficiency for 20 mg/L of the AO7 solution was achieved, when the doping content, pH of precursor fluid, catalyst dosage was GB30, pH = 9, 200 mg, respectively. A series of free radical trapping experiments showed that $^{\bullet}O_2^-$ played the most important role in the degradation of AO7. The enhanced catalytic activity of the $BiVO_4$/RGO composite can be attributed to the RGO. As an electron acceptor and transporter, RGO can effectively promote charge transfer in composite and inhibit the recombination of photoelectron-hole pairs.

Acknowledgment

The authors gratefully acknowledge the financial support provided by Shaanxi Natural Science Foundation (Grant No. 2021JM-109), the Overseas Student's Science and Technology Activities Project Merit Funding of Shaanxi and the Fundamental Research Funds for the Central Universities (Grant No. 2452017106).

References

[1] H.B. Li, G.C. Liu, X.C. Duan, Monoclinic $BiVO_4$ with regular morphologies: hydrothermal synthesis, characterization and photocatalytic properties, Mater. Chem. Phys., 115 (2009) 9–13.

[2] M.N. Chong, B. Jin, C.W.K. Chow, C. Saint, Recent developments in photocatalytic water treatment technology: a review, Water Res., 44 (2010) 2997–3027.

[3] T.F. Li, T.C. Wang, G.Z. Qu, D.L. Liang, S.B. Hu, Synthesis and photocatalytic performance of reduced graphene oxide-TiO_2 nanocomposites for Orange II degradation under UV light irradiation, Environ. Sci. Pollut. Res., 24 (2017) 12416–12425.

[4] D.B. Zeng, C.L. Yu, Q.Z. Fan, J.L. Zeng, L.F. Wei, Z.S. Li, K. Yang, H.B. Jia, Theoretical and experimental research of novel fluorine doped hierarchical Sn_3O_4 microspheres with excellent photocatalytic performance for removal of Cr(VI) and organic pollutants, Chem. Eng. J., 391 (2020)123607, doi: 10.1016/j.cej.2019.123607.

[5] W. Liu, Y.Q. Yu, L.X. Cao, G. Su, X.Y. Liu, L. Zhang, Y.G. Wang, Synthesis of monoclinic structured $BiVO_4$ spindly microtubes in deep eutectic solvent and their application for dye degradation, J. Hazard. Mater., 181 (2010) 1102–1108.

[6] A.P. Zhang, J.Z. Zhang, Effects of europium doping on the photocatalytic behavior of $BiVO_4$, J. Hazard. Mater., 173 (2010) 265–272.

[7] S. Teyyebah, T. Ahmad, L. Byeong-Kyu, Efficient promotion of charge separation with reduced graphene oxide (rGO) in $BiVO_4$/rGO photoanode for greatly enhanced photoelectrochemical water splitting, Sol. Energy Mater. Sol. Cells, 185 (2018) 325–332.

[8] Y. Li, Z.H. Sun, S.M. Zhu, Y.L. Liao, Z.X. Chen, D. Zhang, Fabrication of $BiVO_4$ nanoplates with active facets on graphene sheets for visible-light photocatalyst, Carbon, 94 (2015) 599–606.

[9] O.K. Okoth, K. Yan, J. Zhang, Mo-doped $BiVO_4$ and graphene nanocomposites with enhanced photoelectrochemical performance for aptasensing of streptomycin, Carbon, 120 (2017) 194–202.

[10] A.L. Wang, S. Song, Y.B. Zhao, W. Wu, Preparation and characterizations of $BiVO_4$/reduced graphene oxide nanocomposites with higher visible light reduction activities, J. Colloid Interface Sci., 445 (2015) 330–336.

[11] G. Singh, A. Choudhary, D. Haranath, A.G. Joshi, N. Singh, S. Singh, R. Pasricha, ZnO decorated luminescent graphene as a potential gas sensor at room temperature, Carbon, 50 (2012) 385–394.

[12] K. Zhao, X.Q. Yan, Y.S. Gu, Z. Kang, Z.M. Bai, S.Y. Cao, Y.C. Liu, X.H. Zhang, Y. Zhang, Self-powered photoelectrochemical biosensor based on CdS/RGO/ZnO nanowire array heterostructure, Small, 12 (2016) 245–251.

[13] S.B. Gawande, S.R. Thakare, Graphene wrapped $BiVO_4$ photocatalyst and its enhanced performance under visible light irradiation, Int. Nano Lett., 2 (2012) 11–16.

[14] Y. Yan, S.F. Sun, Y. Song, X. Yan, W.S. Guan, X.L. Liu, W.D. Shi, Microwave-assisted in situ synthesis of reduced graphene oxide-$BiVO_4$ composite photocatalysts and their enhanced photocatalytic performance for the degradation of ciprofloxacin, J. Hazard. Mater., 250–251 (2013) 106–114.

[15] X.F. Zhang, S. Chen, X. Quan, H.M. Zhao, Preparation and characterization of $BiVO_4$ film electrode and investigation of its photoelectrocatalytic (PEC) ability under visible light, Sep. Purif. Technol., 64 (2008) 309–313.

[16] F.Q. Zhou, Y.L. Min, J.C. Fan, Q.J. Xu, Reduced graphene oxide-grafted cylindrical like W doped $BiVO_4$ hybrids with enhanced performances for photocatalytic applications, Chem. Eng. J., 266 (2015) 48–55.

[17] J. Yu, A. Kudo, Effects of structural variation on the photocatalytic performance of hydrothermally synthesized $BiVO_4$, Adv. Funct. Mater., 16 (2006) 2163–2169.

[18] R. Muzyka, M. Kwoka, Ł. Smędowski, N. Díez, G. Gryglewicz, Oxidation of graphite by different modified Hummers methods, New Carbon Mater., 32 (2017) 15–20.

[19] Y.S. Fu, X.Q. Sun, X. Wang, $BiVO_4$-graphene catalyst and its high photocatalytic performance under visible light irradiation, Mater. Chem. Phys., 131 (2011) 325–330.

[20] X. Lin, X.Y. Guo, W.L. Shi, L.N. Zhao, Y.S. Yan, Q.W. Wang, Ternary heterostructured Ag-$BiVO_4$/$InVO_4$ composites: Synthesis and enhanced visible-light-driven photocatalytic activity, J. Alloys Compd., 635 (2015) 256–264.

[21] F. Lin, D.G. Wang, Z.X. Jiang, Y. Ma, J. Li, R.G. Li, C Li, Photocatalytic oxidation of thiophene on $BiVO_4$ with dual co-catalysts Pt and RuO_2 under visible light irradiation using molecular oxygen as oxidant, Energy Environ. Sci., 5 (2012) 6400–6406.

[22] Q.M. Shi, W.R. Zhao, L.H. Xie, J.S. Chen, M. Zhang, Y.J. Li, Enhanced visible-light driven photocatalytic mineralization of indoor toluene via a $BiVO_4$/reduced graphene oxide/Bi_2O_3 all-solid-state Z-scheme system, J. Alloys Compd., 662 (2016) 108–117.

[23] J.B. Wang, C. Liu, S. Yang, X. Lin and W.L. Shi, Fabrication of a ternary heterostructure $BiVO_4$ quantum dots/C_{60}/g-C_3N_4 photocatalyst with enhanced photocatalytic activity, J. Phys. Chem. Solids, 136 (2020) 109164, doi: 10.1016/j.jpcs.2019.109164.

[24] C.Y. Feng, Y.C. Deng, L. Tang, G.M. Zeng, J.J. Wang, J.F. Yu, Y.N. Liu, B. Peng, H.P. Feng, J.J. Wang, Core-shell Ag_2CrO_4/N-GQDs@g-C_3N_4 composites with anti-photocorrosion performance for enhanced full-spectrum-light photocatalytic activities, Appl. Catal., B, 239 (2018) 525–536.

[25] X.Q. Cao, Y. Gu, H.L. Tian, Y.F. Fang, D. Johnson, Z.Y. Ren, C.C. Chen, Y.P. Huang, Microemulsion synthesis of ms/tz-$BiVO_4$ composites: the effect of pH on crystal structure and photocatalytic performance, Ceram. Int., 46 (2020) 20788–20797.

[26] B. Ren, T.C. Wang, G.Z. Qu, F. Deng, D.L. Liang, W.L. Yang, M.S. Liu, In situ synthesis of g-C_3N_4/TiO_2 heterojunction nanocomposites as a highly active photocatalyst for the degradation of Orange II under visible light irradiation, Environ. Sci. Pollut. Res., 25 (2018) 1–12.

[27] G.Q. Zhou, J.Y. Guo, G.W. Zhou, X.K. Wan, H.X. Shi, Photodegradation of Orange II using waste paper sludge-derived heterogeneous catalyst in the presence of oxalate under ultraviolet light emitting diode irradiation, J. Environ. Sci., 47 (2016) 63–70.

[28] Y.Y. Yao, L. Fang, Y.P. Zhu, F.Y. Wei, X.T. Liu, C. Lian, S.B. Wang, Magnetic core-shell $CuFe_2O_4$@C_3N_4 hybrids for visible light photocatalysis of Orange II, J. Hazard. Mater., 297 (2015) 224–233.

[29] H. Moussa, E. Girot, K. Mozet, H. Alem, G. Medjahdi, R. Schneider, ZnO rods/reduced graphene oxide composites prepared via a solvothermal reaction for efficient sunlight-driven photocatalysis, Appl. Catal., B, 185 (2016) 11–21.

[30] P. Wang, J. Wang, X.F. Wang, H.G. Yu, J.G. Yu, M. Lei, Y.G. Wang, One-step synthesis of easy-recycling TiO_2-rGO nanocomposite photocatalysts with enhanced photocatalytic activity, Appl. Catal., B, 132–133 (2013) 452–459.

[31] W.W. Yao, Y.H. Li, D.X. Yan, M. Ma, Z.K. He, S.G. Chai, X.S. Su, F. Chen, Q. Fu, Fabrication and photocatalysis of TiO_2-graphene sandwich nanosheets with smooth surface and controlled thickness, Chem. Eng. J., 229 (2013) 569–576.

[32] M. Lei, N. Wang, L.H. Zhu, C.S. Xie, H.Q. Tang, A peculiar mechanism for the photocatalytic reduction of decabromodiphenyl ether over reduced graphene oxide-TiO_2 photocatalyst, Chem. Eng. J., 241 (2014) 207–215.

[33] X.N. Luan, M.T.G. Wing, Y. Wang, Enhanced photocatalytic activity of graphene oxide/titania nanosheets composites for methylene blue degradation, Mater. Sci. Semicond. Process., 30 (2015) 592–598.